Proceedings of the 42nd IEEE
Conference on Decision and Control
Maui, Hawaii USA, December 2003

FrE10-5

Controllability issues in flapping flight for biomimetic Micro Aerial Vehicles (MAVs)*

Luca Schenato, Domenico Campolo, Shankar Sastry
Department of Electrical Engineering and Computer Sciences
University of California at Berkeley
{lusche|minmo|sastry}@robotics.eecs.berkeley.edu

Abstract— In this paper we explore controllability in flapping flight for Micro Aerial Vehicles (MAVs), inch-size robots capable of autonomous flight. Differently from previous work, we focus on a MAV with very limited wing kinematics and simple input control schemes. In particular, in the first part we show how an MAV provided with a pair of wings, each with a single degree of freedom and passive rotation, can still ensure controllability. This is obtained by combining two ideas. The first idea is to parameterize wing trajectory based on biomimetic principles, i.e. principles that are directly inspired by observation of real insect flight. The second idea is to treat flapping flight within the framework of high frequency control and to apply averaging theory arguments in order to prove controllability. The results obtained set flapping flight as a compelling example of high frequency control present in nature, and shed light on some of the reasons of superior maneuverability observed in flapping flight. Then, in the second part we show that controllability is still guaranteed even when the wing-thorax dynamics is included and the electromechanical structure is driven by a pulse width modulation (PWM) scheme where only its amplitude, period and duty cycle are controllable on a wingbeat-by-wingbeat basis. However, in this case our modeling clearly shows some tradeoffs between controllability and lift generation efficiency, which seem consistent with observations in real insect flight.

I. INTRODUCTION

Unmanned air vehicles, (UAV), have been a very active area of research for both civil and military applications. Despite recent remarkable achievements obtained with fixed and rotary aircrafts [1], their use in many tasks is still limited by their maneuverability and size. In order to overcome these limitations, the extraordinary flight capabilities of insects have inspired the design of small micro aerial vehicles (MAVs) [2], in particular inch size robots with flapping wings mimicking real flying insects [3]. Their unmatched maneuverability, low fabrication cost and small size make them very attractive for cost-critical missions in environments which are impenetrable for larger size UAVs such as helicopters or airplanes. Moreover, the latest progress in insect flight aerodynamics [4] and in micro-technology [5] seem to provide sufficient tools to fabricate flying insect micro-robots.

Despite the aerodynamic mechanisms present during insect flight have been clearly identified [4], little is still know about how insects actually exploit these mechanisms to achieve complex maneuvers such as saccades or hovering. Besides, electromechanical considerations limit the set of feasible wing kinematics configurations and the input control schemes available.

The goal of this paper is to unveil some of the most important features of insect flight from a control point of view, placing particular emphasis on the electromechanical constraints.

Similar to aerial vehicles based on rotary wings, such as helicopter, flying insects control their flight by controlling their attitude and the magnitude of the vertical force [6]. This is accomplished by the controlling the aerodynamic forces and torques generated by the wings during flapping. However, unlike in helicopters, aerodynamic forces on insect wings are highly nonlinear and time-varying during a wingbeat, and the periodic motion of the wings cannot be ignored. As a result, the system dynamics cannot be approximated by a linear time-invariant model, widely adopted in helicopter theory based on quasi-static assumption on the rotary blades.

The motion of the insect is a nonlinear system with forced periodic inputs. On the other hand, the wingbeat frequency is much higher than the dynamics of the insect itself, since flying insects require several wingbeat periods to complete a complex maneuver such as a saccade. Moreover, the wing pattern motion in real insect does not change dramatically from one wingbeat to another wingbeat, even during fast maneuvers. These two facts lie at the core of the control approach for flapping MAVs proposed in [6] [7], which is based on averaging the system with respect to the wingbeat period, and on parameterizing the wing motion according to biomimetically inspired parameters that can be changed on a wingbeat-by-wingbeat basis.

A similar approach based on averaging has been proposed for the control of fish-like locomotion [8] [9], which analogously to flapping flight, is generated by the interaction of oscillatory appendices with a viscous fluid. However, our approach based on wing motion parametrization, which mimics real insect wing motions, leads naturally to a time invariant system where artificial virtual control inputs appear naturally as a simple function of the wing parameters, thus facilitating the synthesis of feedback control design.

Differently from previous work [7], where we considered wings with two degrees of freedom and analog control input to the the thorax-wing actuators, here we focus on a model with very limited wing kinematics and with simple PWM input to the wings actuators. This is motivated by the necessity of simple electromechanical fabrication and highly efficient power transfer from the power supply to the actuators.

This paper is organized as follows. The next section presents a model for the insect flight dynamics, wing aerodynamics and wing motion parametrization. Then it applies averaging theory arguments to reduce the controllability of the nonlinear time-varying system to the controllability of a nonlinear affine time-invariant system. In Section III we propose a simplified model for the wing-thorax electromechanical structure and a simple PWM control input based on electromechanical considerations, and we study their effect on controllability. In the final section we summarize our findings and we suggest future research directions.

II. FLAPPING FLIGHT MODELING

Flight dynamics of flapping insects is still an open area of research [10] [11]. This is primarily due to the difficulties in measuring aerodynamic forces on real flying insects, and in experimentally validating proposed theoretical models. In this work we model the dynamics of a flying insect as a rigid body subject to external forces. Albeit wings do move relative to the insect body, their mass is within $1 - 5\%$ of total insect mass and hence their effect on the insect dynamics is relatively small and can be neglected. Besides, nonholonomic effects are unlikely, since wings move with an almost symmetrical motion. Therefore, we assume that the insect body motion evolves according to the rigid body motion equations subject to external forces relative to its center of mass [12]. The external forces acting on an insect are the aerodynamic forces generated by the wings, the gravity force, and the body viscous drag. Angular viscous torques are not included since they are negligible with respect to the torques generated by aerodynamic forces. Summing
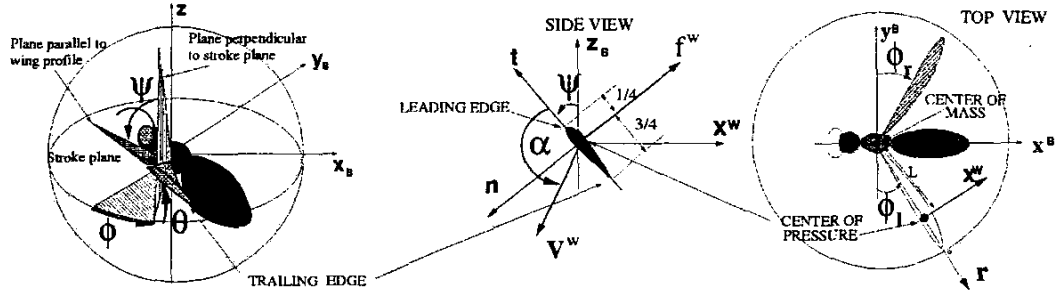
Fig. 1.   Definition of wing kinematic parameters: (*left*) 3D view of left wing, (*center*) side view of wing perpendicular to wing axis of rotation $\vec{r}$, (*right*) top view of insect stroke plane

up, the dynamics of the attitude of a flapping insect are modeled as follows:

$$
\begin{aligned}
\dot{\mathbf{p}}^f &= \mathbf{v}^f \\
\dot{\mathbf{v}}^f &= \tfrac{1}{m}R\mathbf{f}^b - c\mathbf{v}^f - \mathbf{g} \\
\dot{R} &= R\hat{\omega}^b \\
\dot{\omega}^b &= J_b^{-1}(\tau^b - \omega_b \times J_b\omega_b) \\
\hat{\omega}^b &= \begin{bmatrix} 0 & \omega_z{}^b & -\omega_y{}^b \\ -\omega_z{}^b & 0 & \omega_x{}^b \\ \omega_y{}^b & -\omega_x{}^b & 0 \end{bmatrix}
\end{aligned}
\tag{1}
$$

where m is the insect body mass, $\mathbf{p}^f \in \mathbb{R}^3$ and $\mathbf{v}^f \in \mathbb{R}^3$ are the position and velocity of the insect center of mass relative to the fixed frame, respectively, $\mathbf{f}^b$ is the aerodynamic force relative to the body frame B, $c \in \mathbb{R}$ is the viscous damping coefficient, $\mathbf{g}$ is the gravity vector, $\omega^b = [\omega_x{}^b \, \omega_y{}^b \, \omega_z{}^b]^T$ is the angular velocity of the insect body relative to the body frame B, $\tau^b \in \mathbb{R}^3$ is the aerodynamic torque relative to the body frame B attached to the center of mass of the insect body, and $J_b \in \mathbb{R}^{3\times3}$ is the moment of inertia of the insect body relative to the body frame B. The matrix $R \in SO(3) = \{R \in \mathbb{R}^{3\times3} : R^TR = I, \det R = +1\}$ is the rotation matrix representing the orientation of the insect body frame B relative to the fixed frame A. In particular, let $\mathbf{v}^b = [x_b \, y_b \, z_b]^T$ and $\mathbf{v}^a = [x_a \, y_a \, z_a]^T$ the coordinates of a vector $\mathbf{v} \in \mathbb{R}^3$ relative to the body frame B and the fixed frame A, respectively. Then, these coordinates satisfy the transformations $\mathbf{v}_a = R\mathbf{v}_b$ and $\mathbf{v}_b = R^T\mathbf{v}_a$.

The aerodynamic force and torque, $\mathbf{f}^b$ and τ^b, are generated by the motion of the two wings. In insects each wing is quite stiff and can be modeled as a rigid body rotating about its wing base. Let us define a wing frame coordinate system $(\vec{t}, \vec{n}, \vec{r})$ (see Figure 1). The vector $\vec{t}$ is parallel to the wing chord oriented from the trailing to the leading edge. The vector $\vec{n}$ is perpendicular to the wing profile oriented form dorsal to ventral. The vector $\vec{r}$ is oriented from wing base to wing tip. Its position can be defined by three Euler's angles: the stroke angle, ϕ, i.e. a rotation about the $\vec{t}$ axis, the deviation angle from stroke plane, θ, i.e. a rotation about the $\vec{n}$ axis, and the rotation angle, ψ, i.e. a rotation about the $\vec{r}$ axis. The plane swept by the rotation axis $\vec{r}$ when setting the deviation angle θ to zero, is called mean stroke plane. Recent work done by Dickinson and his group [4] unveiled three major mechanisms involved in flapping flight: the delayed stall, the rotational lift, and wake capture. Delayed stall provides most of the aerodynamic force production, while rotational lift and wake capture are present only during wing rotation. In this work, we will consider only the modeling for the delayed stall because the rotational lift and wake capture, besides being mathematically less amenable, have a smaller

contribution in aerodynamic force generation, therefore they are unlikely to change the *qualitative* analysis developed in this work. Indeed, there is evidence that these mechanisms act synergistically with the delayed stall in augmenting force and torque generation while preserving the same "sign" [10]. Experimental results [4] have shown that the delayed stall can be modeled quite accurately by a quasi-steady state equation of instantaneous wing kinematic position and velocity. Its effect is equivalent to apply a vector force perpendicular to the wing profile and on the opposite direction of wing velocity, $\mathbf{v}^w$, at wing center of pressure which is placed at a quarter-chord distance from the leading edge and at a distance of approximately $0.6 - 0.7$ wing-length from the wing base depending on the exact wing shape (see Figure 1). The magnitude of this force is given by:

$$
|\mathbf{f}^w| = \frac{1}{2}\rho_a C_D(\alpha)A_w|\mathbf{v}^w|^2
\tag{2}
$$

where $C_D = C\sin\alpha$ and $C = 3.5$ is the delayed stall force coefficient empirically derived in [4], $\alpha = \cos^{-1}(\vec{t} \cdot \frac{\mathbf{v}^w}{|\mathbf{v}^w|})$ is the angle of attack, A_w is the total wing area, ρ_a is the air density (see Figure 1). Therefore, given the trajectory $(\phi(t), \theta(t), \psi(t))$ for both wings it is possible to compute the total aerodynamic force and torque vectors acting on the center of mass of the insect body as follows:

$$
\begin{aligned}
\mathbf{f}^b(t) &= \mathbf{f}_l^w(t) + \mathbf{f}_r^w(t) \\
\tau^b(t) &= \mathbf{p}_l^w(t) \times \mathbf{f}_l^w(t) + \mathbf{p}_r^w(t) \times \mathbf{f}_r^w(t)
\end{aligned}
\tag{3}
$$

where the subscripts l, r stand for left and right wing, respectively, and $\mathbf{p}^w(t) = L\vec{r}(t)$ is the position of the center of pressure of the wing. Note that $\dot{\mathbf{p}}^w(t) = \mathbf{v}^w(t)$.

Flying insects show a rich set of wing trajectories by varying the stroke angle oscillation from sinusoidal to saw-tooth, by modulating the mean angle of attack during the upstroke and downstroke, by changing the timing of rotation, and by exhibiting out of stroke plane wing motions such as figure-eight and banana-like trajectories [4].

However, in this work we restrict the wings to move on the mean stroke plane, i.e. $\theta(t) = 0$ for both wings, and we assume that wing rotation is instantaneous at the wings inversion of motion maintaining the same angle of attack during upstroke and downstroke, i.e. $\alpha(t) = 45^o$. Also we assume that the wings move at constant angular velocity during the upstroke and the downstroke, i.e. the stroke angle $\phi(t)$ moves according to a sawtooth-like motion as shown in Figure 2. Mathematically, each wing trajectory within a
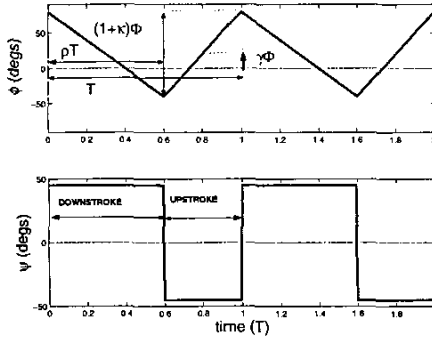
Fig. 2. Wing kinematic during two wingbeat periods: (top) stroke angle, (bottom) rotation angle

single wingbeat is described by the following equations:

$$
\begin{aligned}
\phi(t) &= \begin{cases} A_0(1+\kappa)\left(1 - \frac{2t}{\rho T}\right) + \gamma A_0 & 0 \le t \le \rho T \\ A_0(1+\kappa)\left(2\frac{t-\rho T}{(1-\rho)T} - 1\right) + \gamma A_0 & \rho T < t \le T \end{cases} \\
\psi(t) &= 45^\circ \, \text{sign}(\rho T - t) \qquad\qquad 0 \le t \le T \\
\theta(t) &= 0
\end{aligned}
$$

$$(4)$$

where $\text{sign}(x) = \frac{x}{|x|}$, T is the wingbeat period, A_0 is the stroke amplitude range, κ is a tunable parameter that controls the stroke amplitude, ρ is the ratio of downstroke duration to total wingbeat period, γ is the relative stroke angle offset. We assume that the wingbeat period, T, and the stroke amplitude range, ϕ, are fixed, while the three dimensionless parameters (κ, ρ, γ) can be changed on a wingbeat-by-wingbeat basis. The angle of attack is fixed at 45°, because it is the angle that generates maximum vertical thrust.

Our simplified wing trajectory parametrization is dictated by the necessity of finding feasible wing trajectories for the electromechanical structure, and yet this parametrization should still capture the essence of controllability of real insect flight.

In practice, this particular wing trajectory parametrization based on (κ, ρ, γ) is equivalent to reduce the 3-degree of freedom wing to a single-degree of freedom wing with a passive rotation, i.e. the only degree of freedom that is really controllable is the stroke angle.

In order to simplify analytical derivations of these two vectors, we also assume that the two insect wing bases coincide with the insect center of mass, that the $x^b - y^b$ plane of the body frame is parallel to the mean stroke plane as shown in Figure 1. Therefore, the position of the center of pressure of the wings can be written in cartesian coordinate relative to body frame as $\mathbf{p}_l^w(t) = L(\sin\phi_l(t), -\cos\phi_l(t), 0)$ and $\mathbf{p}_r^w(t) = L(\sin\phi_r(t), \cos\phi_r(t), 0)$

Substituting Equations (4) into Equation (2), the delayed stall force acting on a wing can be written in cartesian coordinate relative to body frame as follows:

$$
\mathbf{f}_l^w(t) = F \begin{bmatrix} -\dot{\phi}_l(t)\,|\dot{\phi}_l(t)|\,\cos[\phi_l(t)] \\ \dot{\phi}_l(t)\,|\dot{\phi}_l(t)|\,\sin[\phi_l(t)] \\ \dot{\phi}_l^2(t) \end{bmatrix} \tag{5}
$$

where $F = \frac{1}{4}\rho_a C A_w L^2$ is a constant, and we used the fact that $\mathbf{v}_w(t) = \dot{\mathbf{p}}^w$ and $\alpha(t) = 45^\circ$. An analogous equation can be written for $\mathbf{f}_r^w(t)$, only the sign in the y-component is flipped. Substituting Equation (5) and its analogous for the

right wing into Equations (3) we obtain the total wrench:

$$
\mathbf{f}^b(t) = F \begin{bmatrix} -|\dot{\phi}_l|\dot{\phi}_l\cos\phi_l - |\dot{\phi}_r|\dot{\phi}_r\cos\phi_l \\ |\dot{\phi}_l|\dot{\phi}_l\sin\phi_l - |\dot{\phi}_r|\dot{\phi}_r\sin\phi_l \\ \dot{\phi}_l^2 + \dot{\phi}_r^2 \end{bmatrix}
$$

$$
\tau^b(t) = FL \begin{bmatrix} \dot{\phi}_l^2\cos\phi_l - \dot{\phi}_r^2\cos\phi_r \\ -\dot{\phi}_l^2\sin\phi_l - \dot{\phi}_r^2\sin\phi_r \\ |\dot{\phi}_l|\dot{\phi}_l - |\dot{\phi}_r|\dot{\phi}_r \end{bmatrix} \tag{6}
$$

If we substitute Equations (6), into Equations (1), we find that the insect dynamics is a twelve-dimensional nonlinear time-varying dynamical system. However, one could notice that the aerodynamic forces and torques are quasi-periodic and that insect requires several wingbeat periods for completing a full maneuver. This means that the insect dynamics is relatively slow with respect to the frequency of aerodynamic forces. At this point we can use averaging theory which shows, loosely speaking, that the trajectory of the averaged dynamics is a good approximation of the true solution as long as the wingbeat frequency is sufficiently large [13] [14]. More precisely, the approximation bounds are stated in following theorem:

Theorem 1. *Let us consider the following systems:*

$$
\begin{cases} \dot{x} &= f(x,u) \\ u &= u(v,t) \\ v &= v(x) \\ u(v,t) &= u(v,t+T) \end{cases} \tag{7}
$$

$$
\begin{cases} \dot{\bar{x}} &= \bar{f}(\bar{x},v) \\ \bar{f}(x,v) &= \frac{1}{T}\int_0^T f(x,u(v,t))dt \\ v &= v(\bar{x}) \end{cases} \tag{8}
$$

where $x, \bar{x} \in \mathbb{R}^n, u \in \mathbb{R}^m, v \in \mathbb{R}^p$, and all functions and their partial derivatives are continuous up to second order.

- *If $\bar{x}(0) - x(0) = O(T)$, then there exists a T^* such that for all $0 < T < T^*$, $x(t) - \bar{x}(t) = O(T)$ over a timescale of order $O(1)$.*
- *If $\bar{x} = 0$ is also an exponentially stable equilibrium point for the averaged system (8), then $x(t) - \bar{x}(t) = O(T)$ for all $t \in [0, \infty)$. Moreover the original system (7) has a unique, exponentially stable, T-periodic limit cycle $x_T(t)$ with the property $\|x_T(t)\| < kT$.*

Given the limited space of this paper, the proof is omitted, and it will be presented in a forthcoming technical paper.

This theorem shows that T-periodic feedback laws can exponentially stabilize a system about a T-periodic limit cycle. At first it might be not clear the advantage of using periodic control feedback laws since one has to find a "good" parametrization for the input $u = u(v,t)$ and the averaged system is still nonlinear, in general. Besides, these feedback laws do not guarantee the convergence to the desired state $x = 0$, but only to a limit cycle that that is $O(T)$ close to the origin. The advantage of high frequency T-periodic feedback laws resides in the fact that the number of independent virtual input $v \in \mathbb{R}^p$ can be larger than the original number of independent input $u \in \mathbb{R}^m$, i.e. $p > m$. In fact, high frequency control can in principle increase the number of virtual input, as shown by Sussmann and Liu in [15] for nonholonomic affine systems. In the case of flapping flight, however, the increased number of virtual inputs arise from the nonaffine nature of the system. In fact, the stroke angles (ϕ_r, ϕ_r) of Equations (6), which play the role of the input u defined in the previous Theorem, appear nonlinearly in the entry of the wrench. The goal of the parametrization in Equation 4 is to move the wings in order to affect independently as many entry of the wrench as possible.

Another advantage of high frequency control is that the origin $x = 0$ might not be an equilibrium point for the

original system, i.e. there is no input $u*$ such that $f(0, u^*) = 0$. Therefore, this type of feedback can stabilize the system closed to the desired state, which is otherwise unfeasible. The distance from the desired state depends on the frequency T of the input. Therefore, if T is a controllable parameter, the error can be made arbitrarily small by reducing the period T. In the rest of this paragraph we show that these two advantages are actually present in insect flapping flight. In particular, we will show that we are able to generate 5 independent virtual input for the averaged system by controlling actively only 2 input, which are the right and left stroke angles (ϕ_r, ϕ_l). Moreover, both the hovering configuration and the cruise flight with constant velocity are not feasible for the original systems, but they can be approximated with feasible trajectories that are $O(T)$ closed and are exponentially stabilizable. The closeness depends on the period T, and it has been shown elsewhere [7] that the error of the approximation is practically undetectable for inch-size insects or smaller. This is consistent with observations of real insects during free flight which do not seem to oscillate about their trajectories. Therefore, it seems that insect flapping flight represent a very compelling example of high frequency control present in nature.

Instead of considering the time-varying system, we study its dynamics averaged over a single wingbeat period, which requires the computation of the mean aerodynamic force, $\bar{\mathbf{f}}^b = \frac{1}{T} \int_0^T \mathbf{f}^b(t)dt$, and torque, $\bar{\tau}^b = \frac{1}{T} \int_0^T \tau^b(t)dt$:

$$\bar{\mathbf{f}}^b = \frac{4FA_0^2}{T^2} \left[\begin{array}{c} \frac{\text{sinc}(\frac{A_0}{4})\cos(\gamma_l A_0)(1+\kappa_l)^2(1-2\rho_l)}{\rho_l(1-\rho_l)} \\ -\frac{\text{sinc}(\frac{A_0}{4})\sin(\gamma_l A_0)(1+\kappa_l)^2(1-2\rho_l)}{\rho_l(1-\rho_l)} \\ \frac{(1+\kappa_l)^2}{\rho_l(1-\rho_l)} \end{array} \right]$$
$$+ \left[\begin{array}{c} \frac{\text{sinc}(\frac{A_0}{4})\cos(\gamma_r A_0)(1+\kappa_r)^2(1-2\rho_r)}{\rho_r(1-\rho_r)} \\ \frac{\text{sinc}(\frac{A_0}{4})\sin(\gamma_r A_0)(1+\kappa_r)^2(1-2\rho_r)}{\rho_r(1-\rho_r)} \\ \frac{(1+\kappa_r)^2}{\rho_r(1-\rho_r)} \end{array} \right] \quad (9)$$

$$\bar{\tau}^b = \frac{4FLA_0^3}{T^2} \left[\begin{array}{c} -\frac{\text{sinc}(\frac{A_0}{4})\cos(\gamma_l A_0)(1+\kappa_l)^2}{\rho_l(1-\rho_l)} \\ \frac{2\text{sinc}(\frac{A_0}{4})\sin(\gamma_l A_0)(1+\kappa_l)^2}{A_0\rho_l(1-\rho_l)} \\ -\frac{(1+\kappa_l)^2(1-2\rho_l)}{\rho_l(1-\rho_l)} \end{array} \right]$$
$$+ \left[\begin{array}{c} \frac{\text{sinc}(\frac{A_0}{4})\cos(\gamma_r A_0)(1+\kappa_r)^2}{\rho_r(1-\rho_r)} \\ -\frac{2\text{sinc}(\frac{A_0}{4})\sin(\gamma_r A_0)(1+\kappa_r)^2}{A_0\rho_r(1-\rho_r)} \\ \frac{(1+\kappa_r)^2(1-2\rho_r)}{\rho_r(1-\rho_r)} \end{array} \right] \quad (10)$$

where $\text{sinc}(x) = \frac{\sin x}{x}$. The equations above can be linearized about the symmetric wing motions corresponding to $\rho_l = \rho_r = \frac{1}{2}, \gamma_l = \gamma_r = \kappa_l = \kappa_r = 0$. To further simplify results, let define the following input parameter:

$$\begin{aligned} w_1 &= -\text{sinc}(\tfrac{A_0}{4})[(\rho_l - \tfrac{1}{2}) + (\rho_r - \tfrac{1}{2})] \\ w_2 &= \kappa_l + \kappa_r \\ w_3 &= -\text{sinc}(\tfrac{A_0}{4})[\kappa_l - \kappa_r] \\ w_4 &= -\text{sinc}(\tfrac{A_0}{4})[\gamma_l + \gamma_r] \\ w_5 &= (\rho_l - \tfrac{1}{2}) - (\rho_r - \tfrac{1}{2}) \end{aligned} \quad (11)$$

to obtain:

$$\bar{\mathbf{f}}^b = f_0 \left[\begin{array}{c} 0 \\ 0 \\ 1 \end{array} \right] + f_0 \left[\begin{array}{c} w_1 \\ 0 \\ w_2 \end{array} \right], \quad \bar{\tau}^b = \tau_0 \left[\begin{array}{c} w_3 \\ w_4 \\ w_5 \end{array} \right] \quad (12)$$

where $f_0 = \frac{32FA_0^2}{T^2}$ and $\tau_0 = \frac{32FLA_0^3}{T^2}$. Note that the mean stroke amplitude A_0 and wingbeat period T can be chosen to exactly balance the gravity force mg, i.e. $f_0 = mg$. The

linearized wrench clearly show how the kinematic parameters can be combined to control *independently* all the forces and torques about the insect center of mass, except for the force component along the y-direction of the body frame. In particular, a difference in amplitude in the two wings would result in a net roll torque, the increase in amplitude of both wing would results in a larger vertical thrust. A difference in speed between downstroke and upstroke on both wing leads to a net forward thrust, while a difference in speed between the two wings leads in a net yaw torque. Finally, an analogous change in the offset of stroke motion on both wings gives rise to a net pitch torque. Equation (11) can be thought as a linear map $B \in \mathbb{R}^{5 \times 6}$ from the wing kinematic parameters, $\nu = (\rho_l, \kappa_l, \gamma_l, \rho_r, \kappa_r, \gamma_r)$, to the virtual control inputs $w = (w_1, w_2, w_3, w_4, w_5)$, i.e. $w = B\nu$. Although the map B is not invertible since it is not a square matrix, it is always possible to find a linear map $B^\dagger \in \mathbb{R}^{6 \times 5}$ such that, for any vector w the vector $\nu = B^\dagger w$, satisfies $w = BB^\dagger w$, i.e. $BB^\dagger = I_{5 \times 5}$. One natural choice is to use the pseudoinverse of the matrix B, i.e. $B^\dagger = (B^T B)^{-1} B^T$. It is clear that the wing kinematic parametrization chosen in Equations (4) is sufficient to move the insect in any direction, since it is possible to synthesize feedback laws based on the input control vector w, and then use the static map $B^\dagger$ to find the corresponding wing kinematic parameters ν. Moreover, Equations (4) shed light on some of the reasons for the superior maneuverability of insect flight. In fact, differently from helicopter-like vehicles, flapping insects can generate forward or backward thrust forces without necessarily pitch the body orientation, thus resulting more responsive during hovering mode and in initiating forward flight from rest.

We can summarize our results in the following theorem:

Theorem 2. *Define the system $\dot{x} = f(x, u)$ given by Equations (1) and (6), where $x = (\mathbf{p}^f, \mathbf{v}^f, R, \omega_b)$ and $u = (\phi_l, \phi_r)$. Let the control input $u = u(v, t)$ be parameterized as in Equations (4) and T-periodic, where $v = (\rho_l, \kappa_l, \gamma_l, \rho_r, \kappa_r, \gamma_r)$ are the wing kinematic parameters. The corresponding averaged system $\dot{\bar{x}} = \bar{f}(\bar{x}, v) = \frac{1}{T} \int_0^T f(\bar{x}, u(v, t))dt$ is given by Equations (1), (9) and (10).*

1) *The averaged system, $\dot{\bar{x}} = \bar{f}(\bar{x}, v)$, is locally accessible*
2) *The hovering configuration $\mathbf{q} = (\mathbf{p}^j, \mathbf{v}^j, R, \omega_b) = (P_0, 0, I_{3 \times 3}, 0)$, where $P_0 \in \mathbb{R}^3$ is an arbitrary point in space, is an equilibrium point for the averaged system $\dot{\bar{x}} = \bar{f}(\bar{x}, \nu)$, and its linearization is controllable.*
3) *The motion of the center of mass along a straight line with constant velocity, i.e. $\mathbf{v}^j(t) = \mathbf{v}^*$ where $\mathbf{v}^* \in \mathbb{R}^3$ is constant, is a feasible trajectory for the the averaged system $\dot{\bar{x}} = \bar{f}(\bar{x}, \nu)$ and it is controllable about this trajectory.*
4) *The original system $\dot{x} = f(x, u)$ can be exponentially stabilized about a T-periodic limit cycle $x_T(t)$. In particular there are limit cycles with the property $\|x_T(t) - x^*(t)\| < kT$ where $x^*(t)$ can be the hovering configuration or the motion along a straight line with constant velocity.*

Given the limited space of this paper, the proofs are omitted, and they will be presented in a forthcoming technical paper.

In other words, this theorem states that the averaged dynamics is a good approximation for sufficiently high wingbeat frequency, therefore designing exponentially stabilizing control laws for the averaged dynamics would result in stable dynamics for the true system. The fact that the system is globally accessible is quite intuitive since it is possible to control altitude by modulating the vertical thrust generation, and $x - y$ position by steering the body orientation similarly to helicopters. In practice, accessibility is a necessary condition to be able to find a control input that can steer the insect

from any initial configuration to any final configuration. This is very important when designing complex maneuvers such as saccades, take off and landing. Finally, stabilizing control laws for hovering and cruising flight modes, two fundamental building blocks for high performance flight, can be readily synthesized from the linearized averaged wrench described by Equations (12). In particular, linear feedback laws, i.e. $v = Kx$, can be designed to (locally) stabilize flight, which is critical to MFIs because of their limited computational capabilities.

III. THORAX TOY MODEL

A simplified model of the actuator-thorax-wing system is derived here. As shown in [16], the piezoelectric actuator can be seen as a pure force generator with a parallel stiffness, where the output force is proportional to the input voltage $v(t)$. The thorax, basically consisting of a 4-bar mechanism, is deployed to transform the force/linear displacement at the tip of the actuator into torque/angular displacement at the base of the wing. The wing will contribute to the dynamics with its rotary inertia and its aerodynamic damping. In order to underline the principal features of flapping flight, a simplified electromechanical model will be used. A detailed model for a 2 degrees of freedom (d.o.f.) thorax-wing can be found in [17], while here only 1 d.o.f. will be considered, as the one sketched in Figure 3, where the rotation along the wing axis is passive, i.e. the trailing edge of the wing simply follows the leading edge (see Figure 1). With reference to Figure 3, the thorax transmission will be modelled as a static linear relation, i.e. nonlinearities at high fields will be neglected, and the aerodynamic damping will be considered as a linear function of the wing speed, although a more faithful model would consider a quadratic dependence on the wing speed as suggested by Equation (2).
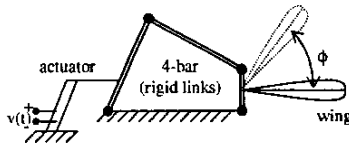

Fig. 3. Actuator, 4-bar, wing system.

In [16] is shown how to relate geometrical and physical characteristics of actuator-thorax-wing system to the parameters that characterize a second order systems, i.e. DC gain K_{DC}, resonant frequency ω_n and quality factor Q. The actual values for these parameters have been choosen based on those experimentally observed on blowflies, our target size MFI. In fact, the actuator stiffness is tuned with wing inertia and the thorax transmission ratio ([17], [16]) in order to resonate at $150Hz$, i.e. $\omega_n = 2\pi 150 \ rad/sec$, while the quality factor is typically $Q = 3$, as shown in [16].

Let $v(t)$, $\phi(t)$ and $\dot{\phi}(t)$ be respectively the input voltage, the output wing displacement and the output wing speed and V, Φ and $\dot{\Phi}$ be their Laplace transforms. The dynamics of the second order system in the time domain are determined by:

$$\begin{bmatrix} \dot{\phi}(t) \\ \ddot{\phi}(t) \end{bmatrix} = \begin{bmatrix} 0 & 1 \\ -\omega_n^2 & -\frac{\omega_n}{Q} \end{bmatrix} \begin{bmatrix} \phi(t) \\ \dot{\phi}(t) \end{bmatrix} + \begin{bmatrix} 0 \\ K_{DC} \end{bmatrix} v(t)$$

(13)

while in the Laplace domain it can be expressed as:

$$\begin{bmatrix} \Phi \\ \dot{\Phi} \end{bmatrix} = \frac{K_{DC} \ \omega_n^2}{s^2 + \frac{\omega_n}{Q}s + \omega_n^2} \begin{bmatrix} 1 \\ s \end{bmatrix} V = \begin{bmatrix} F(s) \\ \dot{F}(s) \end{bmatrix} V \quad (14)$$

A. Controllability via Pulse Width Modulation

In this section the case of symmetric wing kinematics will be considered in order to highlight the key aspects of controllability by means of simplified calculations. Since the wings move with symmetric motion, the force along the y-axis and the roll and yaw torques generated by the left wing are exactly balanced by the right wing, therefore the dynamics of the insect is constrained to the x-z plane. Formally, the simplified system is described by the equations:

$$\begin{bmatrix} m\ddot{p}_x^f \\ m(\ddot{p}_z^f + g) \\ J_y^b \ddot{\vartheta} \end{bmatrix} = \begin{bmatrix} \cos(\vartheta) & -\sin(\vartheta) & 0 \\ \sin(\vartheta) & \cos(\vartheta) & 0 \\ 0 & 0 & 1 \end{bmatrix} \begin{bmatrix} f_x^b \\ f_z^b \\ \tau_z^b \end{bmatrix}$$
(15)

where m is the insect mass, J_y^b is its inertia relative to the y-axis (see Figure 1), ϑ is pitch angle, and g is the gravity.

In a previous section, forces and torque were derived after parameterizing wing kinematics with input parameters (κ, ρ, γ). Here the motion of the wings is determined by the wing-thorax electromechanical system driven by a piezoelectric actuator. A piezoelectric actuator is capable of transforming an input voltage into an output mechanical displacement. Its parasitic capacitance mainly affects the efficiency of such a conversion [18]. Due to energy/size constraints [16], a binary input voltage ($\pm V_0$), i.e. a switching stage, will be employed. It is important to limit the number of switches per cycle because each switch lead to unavoidable losses [18] and for this reason only square waves with variable duty cycle will be considered. Therefore a PWM will be employed and the input parameters will be related to the input voltage $v(t)$, i.e. its amplitude V_0, its frequency ω_0 and its duty cycle d, as follows:

$$v(t) = V_0 \, \text{sign}(dT - t) \qquad 0 \le t \le T \qquad (16)$$

where $T = \frac{2\pi}{\omega_0}$.

In order to control the system (15), we should be able to vary input parameters (V_0, ω_0, d) so that the wrench $[f_x^b \ f_z^b \ \tau_z^b]^T$ might assume any value (within an open ball around the origin). From Equation (13), $\phi(t)$ depends linearly on V_0 and then the forces will depend linearly on V_0^2 which can be used to modulate the wrench modulus. What is left to be shown is how ω_0 and d can modulate the wrench direction. When only steady state is of interest, $v(t)$, $\phi(t)$ and $\dot{\phi}(t)$ can be expanded as Fourier series. For a generic function $w(t)$:

$$w(t) = W_{DC} + \sum_{n=1}^{\infty} |W_n| \cos(n\omega_0 t + \Theta(W_n)) \qquad (17)$$

where ω_0 is the input frequency, usually centered around ω_n, W_{DC} is the DC component of $w(t)$, W_n is the (generally a complex number) Fourier coefficient, and $|W_n|$ and $\Theta(W_n)$ represent respectively its modulus and phase.

$v(t)$	$\phi(t)$	$\dot{\phi}(t)$
$2V_0(d - \frac{1}{2})$	$K_{DC} \, 2V_0(d - \frac{1}{2})$	0
$2\frac{\sin(\pi d n)}{\pi n}$	$2\frac{\sin(\pi d n)}{\pi n}F(n\,j\omega_0)$	$2\frac{\sin(\pi d n)}{\pi n}\dot{F}(n\,j\omega_0)$

TABLE I

FOURIER COEFFICIENTS FOR $v(t)$, $\phi(t)$, AND $\dot{\phi}(t)$.

Considering $v(t)$ as a (periodic) square wave of amplitude $\pm V_0$ and duty cycle d, steady state solutions of (14) can be derived at once by simply posing $s = j\omega$ as shown in Table I where the first row refers to the DC component while the second row refers to n-th coefficient of the Fourier series, i.e. $s = n\,j\omega_0$.

Since the purpose is driving with square-waves, next it will be shown how, starting with a nominal square-wave of frequency $\omega_0 = 2\pi 150 rad/sec$ and duty cycle $d = 0.5$, variations of the input frequency and duty cycle can provide enough degrees of freedom to adjust the mean wrench:

$$\begin{bmatrix} \overline{f}_z^b \\ \overline{f}_x^b \\ \overline{\tau}_y^b \end{bmatrix} = \frac{F}{T} \int_0^T \begin{bmatrix} \dot{\phi}^2 \\ -\dot{\phi}|\dot{\phi}|\cos\phi \\ \dot{\phi}^2\sin\phi \end{bmatrix} dt \qquad (18)$$

where $T = 2\pi/\omega_0$ and F has been defined in the previous section.

Considering the state space $\phi - \dot{\phi}$, periodic trajectories will determine closed loops. Integrals in Equation (18), after a change of variables ($d\phi = \dot{\phi}\,dt$), will solely depend upon the trajectory in the state space. For instance, $\overline{\tau}_y^b$ will correspond to the area enclosed by a trajectory divided by T.
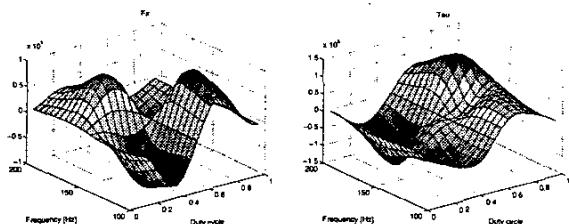

Fig. 4. (left) Mean force in the x direction (body frame) versus input frequency (nominal $150Hz$) and duty cycle (nominal 0.5). (right)
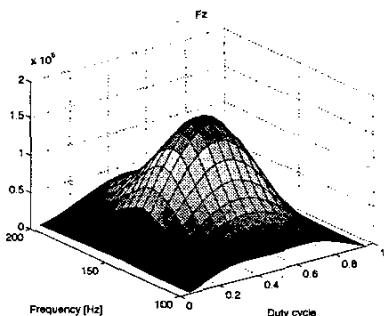

Fig. 5. Mean force in the z direction (body frame) versus input frequency (nominal $150Hz$) and duty cycle (nominal 0.5).

Consider the plane of input parameters (ω_0 and d) centered around their nominal values ($150Hz$ and 0.5). From Figure (4) it is clear that, given any two desired values for $\overline{f}_x^b$ and $\overline{\tau}_y^b$ in a (small) neighborhood of zero, it is always possible to find an input frequency and duty cycle that will provide those outputs. It is in fact possible to distinguish 4 quadrants where mean torque and mean force along x-axis assume arbitrary sign:

input quadrant	$\overline{f}_x^b$	$\overline{\tau}_y^b$
$\omega_0 > 2\pi 150,\ d > 0.5$	$-$	$+$
$\omega_0 < 2\pi 150,\ d > 0.5$	$+$	$+$
$\omega_0 < 2\pi 150,\ d < 0.5$	$-$	$-$
$\omega_0 > 2\pi 150,\ d < 0.5$	$+$	$-$

Note how, although mean torque and mean x-axis force change sign at each quadrant, z-axis mean force does not

change significantly since the nominal values of input frequency and duty cycle correspond to a maximum of $\overline{f}_z^b$, as shown in Figure (5).

During hovering, the z-axis of the body frame and the z-axis of the fix frame are almost aligned. Because of gravity, only positively directed z-axis components of the force are of interest. A simple way to obtain a negative z-axis force is by decreasing power to the wings, i.e. lowering $|\dot{\phi}|^2$. This can easily be accomplished in the stage (generally a DC-DC converter [18]) that is used to generate the high driving voltage ($\pm V_0$) for the piezoelectric actuators. The analysis in this section can be summarized by saying that there exists a nonlinear *locally invertible* map $\Pi : (V_0, d, \omega_0) \rightarrow (w_1, w_2, w_3)$ such that:

$$\begin{bmatrix} \overline{f}_z^b \\ \overline{f}_x^b \\ \overline{\tau}_y^b \end{bmatrix} = \begin{bmatrix} mg \\ 0 \\ 0 \end{bmatrix} + \begin{bmatrix} w_1 \\ w_2 \\ w_3 \end{bmatrix} \qquad (19)$$

Equation (19) is analogous to Equation (12) and the map Π in analogous to the linear map B of Equation (11), therefore similar considerations about controllability and synthesis of feedback control laws can be derived.

B. Input-Output Delay

Whatever the control law will be, input frequency and duty cycle shall certainly vary much "slowly" with respect to the wing beat period $T = 2\pi/\omega_0$. It is important to determine what "slowly" means in this case. For this reason an estimate will be derived of the time delay occurring between the setting of input (frequency and/or duty cycle) and the generation of a steady output (the desired mean forces or mean torque).

Suppose the control law decides to switch at time $t = 0$ from an initial steady state space trajectory $[\phi(t) \ \dot{\phi}(t)]^T$ relative to input variables (V_0, ω_0, d) to a new one relative to (V_0', ω_0', d'). Accordingly to linear systems theory, the trajectory after time $t = 0$ can be thought of the superposition of the steady state trajectory $[\phi'(t) \ \dot{\phi}'(t)]^T$ and a transient trajectory $[\Delta\phi(t) \ \Delta\dot{\phi}(t)]^T$.

Both initial and final steady state trajectories can easily be determined by Fourier coefficients in Table I. The transient is determined by the evolution of the system with initial conditions (at time $t = 0$) $[\phi(0) - \phi'(0) \ \dot{\phi}(0) - \dot{\phi}'(0)]^T = [\Delta\phi(0) \ \Delta\dot{\phi}(0)]^T$ and zero input voltage.

Two steady state trajectories, corresponding to inputs (V_0, ω_0, d) and (V_0', ω_0', d'), are used to evaluate integrals in Equation (18). The time it takes for such integrals to stabilize around the final value is exactly the time it takes for the transient $[\Delta\phi(t) \ \Delta\dot{\phi}(t)]^T$ to fade away. Such a decay simply depends on $[\Delta\phi(0) \ \Delta\dot{\phi}(0)]^T$ and the eigenvalues of the second order system in Equation (14), i.e. in the state space variables:

$$\frac{d}{dt}\begin{bmatrix} \Delta\phi(t) \\ \Delta\dot{\phi}(t) \end{bmatrix} = \begin{bmatrix} 0 & 1 \\ -\omega_n^2 & -\frac{\omega_n}{Q} \end{bmatrix}\begin{bmatrix} \Delta\phi(t) \\ \Delta\dot{\phi}(t) \end{bmatrix} \qquad (20)$$

with eigenvalues:

$$\lambda = \omega_n\frac{-1 \pm \sqrt{1 - 4Q^2}}{2Q} \approx -\frac{\omega_n}{2Q} \pm j\omega_n \qquad (21)$$

approximation clearly holds for $Q = 3$. The purely imaginary term represents the oscillatory nature of the filter while the real one represents its damping. The inverse of the real term is the time constant, i.e. $2Q/\omega_n = TQ/\pi < T$ when $Q = 3 < \pi$. The time constant is less than a period (the period of the input voltage is close to the period of the

resonant frequency of the filter). In Figure (6), average forces and torque settle to steady values within a cycle. Steady values can be derived also from maps in Figure (4), (4) and (5) for input frequencies equal to $140, 150, 165Hz$ and duty cycles equal to $0.4, 0.5$ and 0.6. For smoother transitions, the oscillations can be greatly reduced.
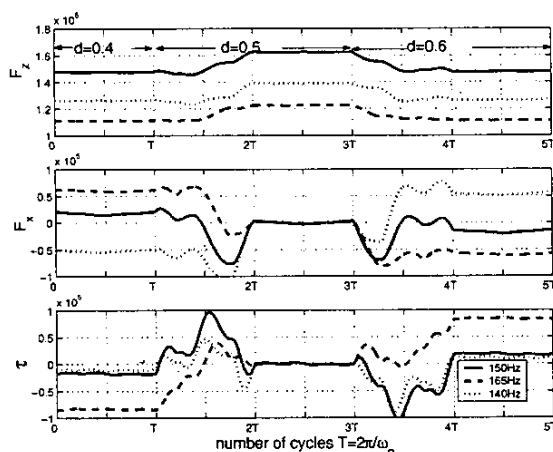

Fig. 6. Averages forces and torque transient due to variation of duty cycle at different frequencies.

As a final remark, it is important to notice how the choice of Q, in the design of the electromechanical system, affects controllability. Previous calculations show how a lower Q implies a quicker decay of transients, i.e. for a given input transition the delay between initial and final values of average forces and torque is lower.

On the other hand, a high Q system would be capable of generating higher forces, including the mean lift f_0, defined in Equation (12), which can be shown to be inversely proportional to the square of Q. Since at present no quantitative analysis for this trade off is available, $Q = 3$ has been chosen based on values observed in most insect species [16].

IV. CONCLUSIONS

In this paper, we presented a detailed controllability analysis of flapping flight for an MAV with limited kinematics and PWM control of wing-thorax electromechanical structure.

In particular, we show that a pair of wings with a single degree of freedom and passive rotation are sufficient to ensure controllability of insect flight for hovering and forward motions. This has been shown using high frequency control theory applied to nonaffine control systems. Besides, the wing parametrization adopted can be readily mapped to the mean torque and forces relative to the body frame, thus posing the basis for simple linear feedback laws. This is extremely valuable given the limited computational power available on board on the MAV. Even in the more realistic scenario when the electromechanical model of the wing-thorax is introduced and a simple PWM control of the actuators is assumed, controllability is still ensured. However, in this case, the wing-thorax electromechanical structure must be designed to have a fast transient decay when control input changes at the beginning of every wingbeat. Interestingly, this condition sets a trade off between controllability and efficiency in lift generation, and it seems to be present also in most flight insects, since the quality factor Q, which regulate this tradeoff, is approximately $1 - 5$ for most species.

This work sets the basis for interesting future research directions. One direction is to introduce a more realistic model for the wing-thorax structure, including a nonlinear

term in the restoring force and a quadratic dependence on the velocity in the damping term, and study their consequences. Another interesting topic is to model the transient decay in the mean forces arising from the dynamics of the wing-thorax structure. Also, we would like to quantify analytically the performance loss in terms of controllability and power efficiency when a single degree of freedom wing with PWM control of actuators is compared to a two-degree of freedom wing with analog control of actuators. Finally, we would like to set up a general framework for designing optimal control input parametrizations given the constraints on the electromechanical structure, and to compare them with those based on biomimetic principles, i.e. those observed in real insects.

V. REFERENCES

[1] H.J. Kim, D.H. Shim, and S.Sastry. A flight control system for aerial robots: Algorithms and experiments. *IFAC Jounrnal of Control Engineering Practice*, 2003. to appear.

[2] B. Motazed, D. Vos, and M. Drela. Aerodynamics and fight control design for hovering MAVs. In *Proc of American Control Conference*, Philadelphia, PA, June 1998.

[3] R.S. Fearing, K.H. Chiang, M.H. Dickinson, D.L. Pick, M. Sitti, and J. Yan. Transmission mechanism for a micromechanical flying insect. In *Proc. of ICRA*, 2000.

[4] M.H. Dickinson, F.O. Lehnmann, and S.S. Sane. Wing rotation and the aerodynamic basis of insect flght. *Science*, 284(5422):1954–1960, 1999.

[5] J. Yan, R.J. Wood, S. Avadhanula, R.S. Fearing, and M. Sitti. Towards flapping wing control for a micromechanical flying insect. In *Proc of the IEEE International Conference on Robotics and Automation*, pages 3901–3908, Seoul, South Korea, May 2001.

[6] L. Schenato, X. Deng, and S.S. Sastry. Flight control system for a micromechanical flying insect. In *Proc of the IEEE International Conference on Robotics and Automation*, Soul, South Korea, May 2002.

[7] X. Deng, L. Schenato, and S. Sastry. Attitude control for a micromechanical flying insect including thorax and sensor models. In *Proc of the IEEE International Conference on Robotics and Automation*, Taipei, Taiwan, May 2003.

[8] K.A. Morgansen, V. Duindam, R.J. Mason, J.W. Burdick, and R.M. Murray. Nonlinear control methods for planar carangiform robot fi sh locomotion. In *Proc of the IEEE International Conference on Robotics and Automation*, Seoul, South Korea, May 2001.

[9] Patricio Velo, Kristi Morgansen, and Joel W. Burdick. Trajectory stabilization for a planar carangiform fi sh. In *Proc of the IEEE International Conference on Robotics and Automation*, Washington DC, U.S.A, May 2002.

[10] S. P. Sane and M. H. Dickinson. The control of flght force by a flapping wing: Lift and drag production. *Journal of Experimental Biology*, 204(204):2607–2626, June 2001.

[11] S. P. Sane and M. H. Dickinson. The aerodynamic effects of wing rotation and a revised quasi-steady model of flapping flght. *Journal of Experimental Biology*, 205:1087–1092, 2002.

[12] R.M. Murray, Z. Li, and S.S. Sastry. *A Mathematical Introduction to Robotic Manipulation*. RCR Press, New York, 1993.

[13] J.A. Sanders and F. Verhulst. *Averaging methods in Nonlinear Dynamical Systems*. Springer-Verlag, New York, N.Y., 1985.

[14] H.K. Khalil. *Nonlinear Systems*. Prentice Hall, Upper Saddle River, N.J., 2000.

[15] H.J. Sussmann and W Liu. Limits of highly oscillatory controls and the approximation of general paths by admissible trajectories, 2001.

[16] M. Sitti, D. Campolo, J. Yan, R.S. Fearing, T. Su, D. Taylor, and T. Sands. Development of pzt and pzn-pt based unimorph actuators for micromechanical flapping mechanisms. In *Proc of the IEEE International Conference on Robotics and Automation*, pages 3839–3846, Seoul, South Korea, May 2001.

[17] S. Avadhanula, R.J. Wood, D. Campolo, and R.S. Fearing. Dynamically tuned design of the mfi thorax. In *Proc of the IEEE International Conference on Robotics and Automation*, Washington, DC, May 2002.

[18] Domenico Campolo, Metin Sitti, and Ronald S. Fearing. Effi cient charge recovery method for driving piezoelectric actuators with quasi-square waves. *IEEE Transaction on Ultrasonics, Ferroelectrics, and Frequency Control*, to appear 2003.